Am J Clin Exp Urol 2024;12(4):149-161
www.ajceu.us /ISSN:2330-1910/AJCEU0158034

Original Article

The aryl hydrocarbon receptor agonist ITE reduces inflammation and urinary dysfunction in a mouse model of autoimmune prostatitis

Robbie SJ Manuel[1,2,3], Allison Rundquist[1,3], Marcela Ambrogi[1,3], Brandon R Scharpf[1,2], Nelson T Peterson[1,2], Jaskiran K Sandhu[1], Sneha Chandrashekar[1], Monica Ridlon[1,2], Latasha K Crawford[4], Kimberly P Keil-Stietz[1,2,3], Richard E Peterson[5], Chad M Vezina[1,2,3]

[1]Department of Comparative Biosciences, University of Wisconsin-Madison, Madison, WI, USA; [2]Molecular and Environmental Toxicology Graduate Program, University of Wisconsin School of Medicine and Public Health, Madison, WI, USA; [3]Endocrinology and Reproductive Physiology Program, University of Wisconsin School of Medicine and Public Health, Madison, WI, USA; [4]Department of Pathological Sciences, University of Wisconsin Madison School of Veterinary Medicine, Madison, WI, USA; [5]Division of Pharmaceutical Sciences, University of Wisconsin School of Pharmacy, Madison, WI, USA

Received May 24, 2024; Accepted July 26, 2024; Epub August 25, 2024; Published August 30, 2024

Abstract: Objectives: Prostate inflammation is linked to lower urinary tract dysfunction and is a key factor in chronic prostatitis/chronic pelvic pain syndrome. Autoimmunity was recently identified as a driver of prostate inflammation. Agonists of the aryl hydrocarbon receptor (AHR), a ligand-activated transcription factor, have been used to suppress autoimmunity in mouse models of colitis, rhinitis, and dermatitis, but whether AHR agonists suppress prostate autoimmunity has not been examined. Here, we test whether ITE (2-(1'H-indole-3'-carbonyl)-thiazole-4-carboxylic acid methyl ester), an AHR agonist, suppresses inflammation, allodynia, and urinary dysfunction in a mouse model of experimental autoimmune prostatitis (EAP). Methods: C57BL/6J adult male mice were immunized with rat prostate antigen to induce EAP or TiterMax Gold® adjuvant (uninflamed control). Mice were also treated with ITE (10 mg/kg/day IP) or DMSO (vehicle, 5 mg/kg/day IP) for 6 days. Using the Nanostring nCounter Inflammation Panel, we evaluated the impact of EAP and ITE on prostatic RNA abundance. We validated EAP and ITE-mediated changes in a subset of RNAs by RT-PCR and RNAScope *in situ* RNA detection. Results: EAP appeared to heighten histological inflammation in the dorsal prostate, induced tactile allodynia, and appeared to increase the frequency of non-voiding bladder contractions. ITE mitigated some actions of EAP. EAP changed abundance of 40 inflammation-related RNAs, while ITE changed abundance of 28 inflammation-related RNAs. We identified a cluster of RNAs for which ITE protected against EAP-induced changes in the abundance of *H2-Ab1*, *S100a8*, and *S100a9*. ITE also increased the abundance of the AHR-responsive *Cyp1a1* RNA. Conclusions: These findings support the hypothesis that ITE activates the AHR in the prostate and reduces autoimmune-mediated prostatitis in mice.

Keywords: CP/CPPS, experimental autoimmune prostatitis, AHR, ITE, inflammation, inflammasome, therapeutic strategies, autoimmunity, urology, translational animal models

Introduction

Lower urinary tract dysfunction (LUTD) and chronic prostatitis/chronic pelvic pain syndrome (CP/CPPS) are urological conditions affecting men of advancing age, impose a large healthcare burden, and adversely affect quality of life for millions [1]. Male LUTD is characterized by increased urinary frequency, nocturia, urinary retention, and urinary tract infections [2]. CP/CPPS is a complex syndrome with pelvic pain as its hallmark and it manifests in urinary and sexual dysfunction [3]. LUTD and CP/CPSS pathogenesis are incompletely understood but genetic, environmental, and immunological factors are involved [3, 4]. Prostate inflammation is considered a major driver of LUTD and CP/CPSS [3, 5-7], and autoimmunity is a recognized trigger for prostate inflammation [8].

There are no currently approved therapies for prostate autoimmunity. However, agonists of

https://doi.org/10.62347/PEGK4888

the aryl hydrocarbon receptor (AHR), a ligand activated transcription factor, have been effective in reducing inflammation in preclinical models of several autoimmune diseases, including multiple sclerosis, psoriasis, atopic dermatitis and inflammatory bowel disease [9, 10]. Known or suspected exposure to AHR agonists during adulthood has been linked to a lower rate of benign prostatic hyperplasia diagnoses in some human populations [11-13].

The purpose of this study was to test the hypothesis that an AHR agonist would reduce inflammation and physiological manifestations of autoimmune prostatitis in a preclinical model. Rat prostate antigen was delivered subcutaneously to C57BL/6J adult male mice to induce EAP and control mice received adjuvant alone. Mice were also exposed to the AHR agonist 2-(1'-indole-3'-carbonyl)-thiazole-4-carboxylic acid methyl ester (ITE) (10 milligrams/kilogram/day IP for 6 days) or DMSO (5 milligrams/kilogram/day IP for 6 days, vehicle) [14]. ITE was selected as a representative potent agonist of the mouse AHR [15]. A potential endogenous ligand for the aryl hydrocarbon receptor has potent agonist activity in vitro and in vivo. EAP caused prostate histological inflammation, heightened secondary sensitivity to cutaneous stimuli (allodynia), and appeared to increase non-voiding bladder contractions consistent with bladder instability. ITE reduced the EAP mediated changes to prostate histology and physiology. A gene expression analysis focused on inflammation related genes found that ITE protected against the EAP mediated increase in the abundance of three RNAs that encode proteins involved in inflammatory responses (*H2-ab1*, *S100a8*, and *S100a9*).

Materials and methods

Mice

All experiments were conducted under an approved protocol from the University of Wisconsin Animal Care and Use Committee and in accordance with the National Institutes of Health Guide for the Care and Use of Laboratory Animals. Mice were housed in Udel® polysulfone microisolator cages on racks or in Innocage® disposable mouse cages (Innovive, San Diego, CA) on an Innorack®; room lighting was maintained on 12-hour light and dark cycles; room temperature was typically 20.5 ± 5°C; humidity was 30-70%. Mice were fed 8604 Teklad Rodent Diet (Harlan Laboratories, Madison WI) and feed and water were available ad libitum. Cages contained corn cob bedding. C57BL/6J mice were purchased from Jackson Laboratories (stock no. 000664, Bar Harbor, ME). All end point measurements were collected in male mice ranging from 7-10-week-old with 3-6 mice used per treatment group. The treatment scheme is illustrated in **Figure 1**.

ITE

2-(1*H*-Indol-3-ylcarbonyl)-4-thiazolecarboxylic acid methyl ester (ITE) (Tocris Bioscience, USA. Cat. No. 1803). ITE is an endogenous aryl hydrocarbon receptor (AHR) agonist. ITE was reconstituted in DMSO and prepared in a stock solution for usage and stored at 25°C.

Prostate antigen (PAg) homogenate

Entire prostate glands from male Wistar Rats (12-55 weeks old) were used to prepare antigen extract. Pooled glands were homogenized in phosphate-buffered saline (PBS) at a pH of 7.2 with protease inhibitors [16]. Pooled glands were homogenized with a 40 milliliter Bellco Glass Dounce homogenizer and pushed through a Cole-Parmer PES Sterile Chromatography Syringe Filter (cat. no. EW-15945-52). Homogenate was subsequently centrifuged at 10,000 *g* for 30 minutes, and the supernatant was used as the PAg.

The Qubit Protein Assay from Qubit™ Protein and Protein Broad Range (BR) Assay Kits (cat. no. Q33211) were used per manufacturer's instructions. Protein concentration was determined for pooled PAg samples and adjusted with sterile water to a concentration of 10 milligrams/milliliter and stored at -80°C until used.

Induction of EAP

Male C57BL/6J mice were injected with 1 milligram of PAg blended in an equal volume of TiterMax® Gold adjuvant (Norcross, GA) with a 26G BD General Use and Precision Glide Hypodermic Needle (0.018in) (Fisher cat. no. 305115), while animals were maintained under isoflurane anesthesia. EAP mice received two subcutaneous injections of equal parts (0.050 milliliters) into the base of tail and the posterior aspect of neck, following a predefined estab-

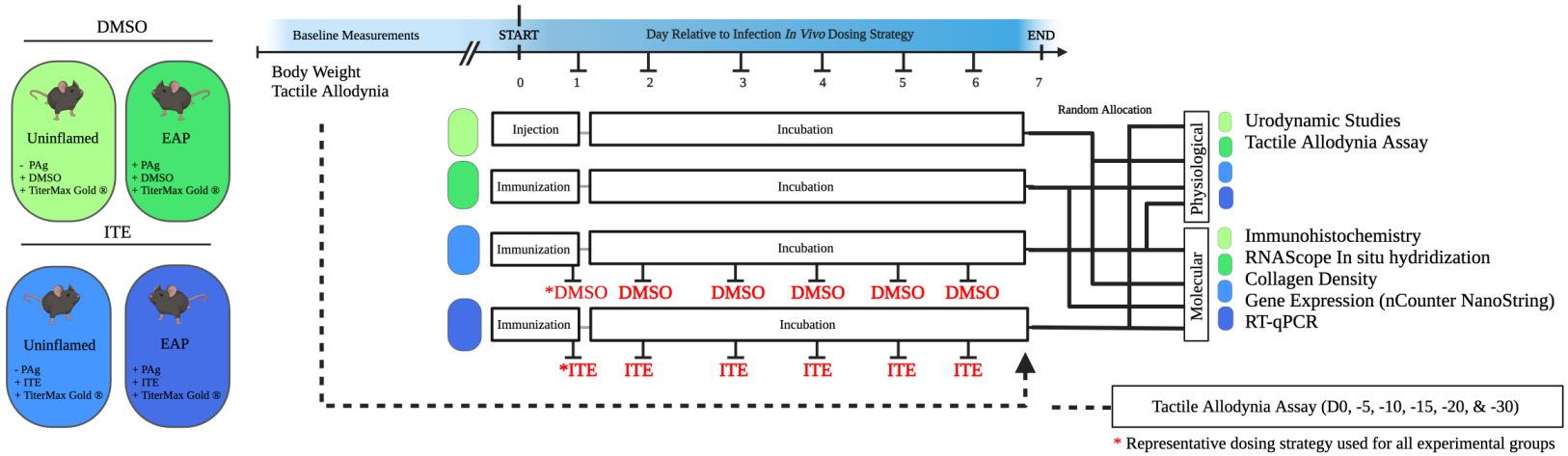

Figure 1. Study design. C57Bl/6J male mice aged 7-9 weeks were used, and randomly selected and placed into one of four experimental groups. A long-term cohort was selected and treated in the same fashion contingent upon experimental group and received VFT testing on D0, -5, -10, -20 and -30 post immunization. All groups received TiterMax Gold Adjuvant for immunization. Vehicle treated animals were dosed with dimethyl sulfoxide (DMSO) with or without combination injection with prostate antigen (PAg). Treatment group received 2-(1'-H-indole-3'carbonyl)-thaizole-4-carboxylic acid methyl ester (ITE) with or without combination injection with prostate antigen (PAg). Groups receiving vehicle and treatment dosing were dosed daily for 6 days. 7 days post immunization, animals were evenly split randomly into physiological or molecular testing groups.

lished protocol [16]. Uninflamed control mice received a subcutaneous injection of TiterMax® Gold Adjuvant only.

Tissue preparation

Seven days after immunization, mice were euthanized by CO_2 asphyxiation. The lower urinary tracts of a subset of mice (5 mice per experimental group) were collected for histological examination. The preparation, fixation, and sectioning of the tissues followed the methods previously outlined [17]. The procedure for removing the lower urinary tract involved severing the ureters where they enter the bladder wall, cutting the vas deferens at its entry point to the bladder neck, and slicing the urethra just above the pubic symphysis. The hemi-dorsal lobes of the prostate were then excised, fixed in a 4% solution of paraformaldehyde, and rinsed with PBS. Prostates were then dehydrated into ethanol, cleared in xylene, and infiltrated with Periplast (Leica Biosystems, Deer Park, IL). Five-micron sagittal tissue sections were mounted on Superfrost Plus Gold Slides (Thermo Fisher Scientific; Waltham, MA).

Reverse transcriptase quantitative-PCR (RT-qPCR)

RT-qPCR was conducted as described previously [18] on dorsal lateral prostate tissue sections with three mice per experimental treatment group using the following gene specific primers and a 60°C annealing temperature: *Cyp1a1*, 5'-TTGTGCCTGCCTCCTACTTTG-3' and 5'-CTCTGAGGCCCAGGTATCTCC-3', *S100a8,* 5'-TGCCGTCTGAACTGGAGAAG-3' and 5'-TGTAGAGGGCATGGTGATTTCC-3', *S100a9,* 5'-TGAGAAGCTGCATGAGAACA-3' and 5'-AAGGCCATTGAGTAAGCCCA-3', and peptidyl prolyl isomerase a (*Ppia*), 5'-TCTCTCCGTAGATGGACCTG-3' and 5'-ATCACGGCCGATGACGAGCC-3'. Relative mRNA abundance was determined by the ΔΔCt method as described previously [18] and normalized to *Ppia* abundance.

Immunofluorescence

Tissues were fixed in 4% paraformaldehyde, dehydrated in alcohol, cleared in xylene, and infiltrated with paraffin. 5 µm sections were generated, mounted on Superfrost™ Plus Gold Slides (Thermo Fisher Scientific; Waltham, MA) and immunolabeled using antibodies against CD45 Monoclonal Antibody (30-F11), eBioscience (Catalog #14-0451-82; 1:100). Non-specific binding sites were blocked for 1 hour in TBSTw containing 1% Blocking Reagent (11096176001, Roche Diagnostics, Indianapolis, IN), 5% normal goat sera, and 1% bovine serum albumin fraction 5 (RGBTw). Tissues were incubated overnight at 4°C with primary antibodies. After several washes with TBSTw, tissues were incubated for 1 hour at room temperature with RGBTw containing 1:250 diluted fluorescent secondary antibodies Anti-Goat 488 (Jackson ImmunoResearch; 711-545-152; 1:500) 2-(4-amidinophenyl)-1H-indole-6-carboxamidine (DAPI) (1:1000) was used to visualize nuclei and slides were mounted in anti-fade media (phosphate-buffered saline containing 80% glycerol and 0.2% n-propyl gallate). Tissue sections were imaged using an Eclipse E600 compound microscope (Nikon Instruments Inc., Melville, NY) fitted with a dry objective (Plan Fluor NA = 0.75; Nikon, Melville, NY) and equipped with NIS elements imaging software (Nikon Instruments Inc.). Fluorescence was detected using DAPI (2-(4-amidinophenyl)-1H-indole-6-carboxamidine), FITC (Chroma Technology Corp, Bellows Fall, VT), filter cube (Nikon, Melville, NY).

In situ detection of RNAs using RNAscope™ multiplex fluorescent reagent kit v2

An RNAscope™ probe against human *H2-ab1* (Catalog #414739; Ventana Systems, Harvard, MA) acquired from Advanced Cell Diagnostics, Inc. (ACD, Hayward, CA). Sections were deparaffinized in xylene, rehydrated, air dried, treated with endogenous hydrogen peroxidase block solution at room temperature for 10 minutes, immersed in pretreatment 2 solution at 100-104°C for 15 minutes, and digested with protease solution for 30 minutes at 40°C. Slides were rinsed with distilled water twice after each step. Probes were then hybridized at 40°C for 2 hours in a humidified chamber. After washing, signal amplification from the hybridized probes was performed by the serial application of amplification solutions per the RNAScope™ instructions. Opal dyes (Akoya Biosciences; Opal 520, FP1487001KT) were reconstituted in dimethylsulfoxide (DMSO) and diluted in tyramide signal amplification buffer (TSA; 1:1000). Horseradish peroxidase (HRP)-C1 and HRP-C2 signals were developed per the RNAscope™ instructions and the slides were counterstained

with DAPI, and cover slipped using antifade mounting media. Slides were imaged as described in the histology and immunostaining section.

Hematoxylin and eosin staining

Hematoxylin and eosin staining was performed by the Histology Service in the School of Veterinary Medicine at the University of Wisconsin-Madison. Stains were imaged using a BZ-X710 digital microscope (Keyence, Itasca, IL) fitted with a 20× objective (PlanFluor, numerical aperture: 0.45).

Mechanical sensitivity testing

The von Frey filament test (VFT) [18] was employed to gauge sensitivity to non-noxious, static tactile stimuli. Mice were acclimated on the testing platform for a minimum of 45 minutes or until they were calm. Calibrated filaments (0.02, 0.04, 0.07, 0.16, 0.4, 0.6, 1, and 1.4 grams) were incrementally applied to the lateral glabrous skin of the hind paw (sural region) until slight buckling of the filament occurred. This process was alternated between hind paws, with each filament presented five times per paw. The tests progressed through all eight filaments, with at least a 1-minute interval between presentations. Testing was paused if mice exhibited activity, resuming once they were calm. Withdrawal of the paw in response to filament pressure was documented as a positive response; the lowest force that elicited a positive withdrawal response was recorded as the mechanical stimulation force threshold. The collected data, inclusive of force thresholds and corresponding behavioral outcomes, constituted the basis for formulating a tactile sensitivity profile specific to each subject animal under scrutiny. The data were analyzed using the UP-Down (UPD)-Reader software, an open-source tool [19].

Cystometry

Anesthetized cystometry was performed as described previously by Kennedy *et al.* [19]. Mice were anesthetized with a subcutaneous injection of urethane (AC32554-0500, Fisher) at a dosage of 1.43 grams urethane/kg mouse. Mice were dosed using a fresh stock solution of urethane in saline at 86 milligrams/milliliter. Mice were placed back into cages for at least 30 minutes prior to beginning surgery. The abdomen was opened, and a purse string suture (6-0 Silk, 501180809, Fisher) placed in the dome of the bladder. PE-50 tubing (NC9140178, Fisher) was used as a catheter and placed into the dome of the bladder using a 25-gauge, 1.5-inch needle. The needle was removed, and the purse string suture tied around the catheter. The body wall and skin were closed with a suture and the mouse was allowed to recover on a heating pad for 60 minutes. Following recovery, mice were connected to an in-line pressure transducer and infusion pump. Saline was infused at a rate of 0.8 milliliters/hour and pressure recorded using an MLT844 physiological pressure transducer (ADInstruments) connected to an FE221 Bridge Amp (ADInstruments) with a Power lab 2/26 (PL2602) data acquisition system.

Cystometrograms were analyzed using LabChart software (ADInstruments). Recordings were conducted for 1 hour or until a steady pattern was achieved. 3-5 consecutive voids were analyzed and averaged per animal and were selected by an individual blinded to treatment conditions. Parameters measured are described in detail previously [20] and include void duration (time between threshold pressure and baseline pressure after a void), void interval (time between baseline pressure to baseline pressure during a void cycle), normalized threshold pressure (threshold pressure - baseline pressure), normalized peak void pressure (peak void pressure - baseline pressure), non-voiding contractions (spikes in pressure before a void not leading to release of urine) and compliance (infused volume/change in pressure (threshold-baseline)).

Gene expression analysis by NanoString profiling

Data was analyzed by ROSALIND® (https://rosalind.bio/), with a HyperScale architecture developed by ROSALIND, Inc. (San Diego, CA). Read Distribution percentages, violin plots, identity heatmaps, and sample MDS plots were generated as part of the QC step. Normalization, fold changes and *p*-values were calculated using criteria provided by Nanostring. ROSALIND® follows the nCounter® Advanced Analysis protocol of dividing counts within a lane by the geometric mean of the normalizer probes from the same lane. Housekeeping

probes to be used for normalization are selected based on the geNorm algorithm as implemented in the NormqPCR R library [21]. Abundance of various cell populations is calculated on ROSALIND using the Nanostring Cell Type Profiling Module. ROSALIND performs a filtering of Cell Type Profiling results to include results that have scores with a *p* value greater than or equal to 0.05. Fold changes and *p* values are calculated using the fast method as described in the nCounter® Advanced Analysis 2.0 User Manual. *P*-value adjustment is performed using the Benjamini-Hochberg method of estimating false discovery rates (FDR). Clustering of genes for the final heatmap of differentially expressed genes was done using the PAM (Partitioning Around Medoids) method using the fpc R. Hypergeometric distribution was used to analyze the enrichment of pathways, gene ontology, domain structure, and other ontologies [21].

Statistical analysis

All data are expressed as mean ± Standard Error of the Mean. Statistical analyses were conducted using GraphPad Prism version 10.0.2 (GraphPad Software, La Jolla, California). The Shapiro-Wilk test was used to evaluate normality of distribution and distributions with a *P* value > 0.05 were normally distributed. Non-normal data underwent transformation (logarithmic or square root) to achieve normality. For NanoString Gene Expression analyses involving multiple t-tests, an FDR approach was utilized to adjust for multiple comparisons. Statistical analysis of multiple, normally distributed groups was conducted using one-way ANOVA followed by Tukey multiple comparisons test. Statistical analysis of multiple groups that were not normally distributed was conducted using the Kruskal-Wallis test followed by Dunn's multiple comparisons test. A *P* value of less than 0.05 was considered a significant difference between or among groups. For the VFT, the determination of a 50% threshold was facilitated by the application of the following equation:

$$50\%\ threshold\ (g) = 10^{Xf + \kappa\delta}/10{,}000$$

50% Threshold = $X_f + \kappa \times \delta$, where X_f denotes the value (in log units) of the final von Frey filament used, κ represents the tabular value corresponding to the pattern of positive/negative responses, and δ signifies the mean difference (in log units) between stimuli as previously described [19].

Results

ITE reduces histological inflammation and partially reduces secondary tactile sensitivity induced by EAP

The prostate is susceptible to various inflammatory and cancerous conditions affecting men across all age groups. Interestingly, inflammation can occur without the presence of infectious agents, indicating the possibility of an autoimmune reaction [22, 23]. While AHR signaling has been shown to reduce autoimmunity in tissues other than the prostate [24], the role of AHR in controlling autoimmune responses within the prostate remains unexplored. We collected and purified adult rat prostate extract (includes dorsolateral, ventral, and anterior prostate lobes, rat prostatic antigen, PAg) as described in the methods and mixed it with TiterMax Gold adjuvant in a 1:1 ratio. EAP mice received two subcutaneous injections of PAg in equal parts. Mice randomly selected to receive ITE were injected in the lower right ventral aspect of the abdomen with 10 milligrams/kilogram/day IP for 6 d. Age-matched control mice were immunized with DMSO and TiterMax Gold adjuvant in a 1:1 ratio. **Figure 1** illustrates the study design. Prostates were collected from a subset of mice (3-5 from each experimental group) seven days after the first immunization and cut to a thickness of five microns for histological analysis. EAP appeared to cause inflammation, characterized by inflammatory infiltration and stromal thickening. Inflammatory infiltration and stromal thickening were visibly less in ITE treated mice (**Figure 2A**, **2B**).

Because prostate inflammation can be painful [25], we used the von Frey Filament Test (VFT) to determine whether EAP drives changes in secondary tactile sensitivity (**Figure 3**). Fibers of increasing stiffness were applied to the lateral plantar region of the hindpaw to evaluate the withdrawal reflex. VFT testing was conducted on the day of immunization and every 5 days for 4 weeks. EAP significantly reduced the withdrawal threshold 5 days post-immunization (P = 0.0174), consistent with the induction of tactile allodynia. This effect was partially blocked by ITE.

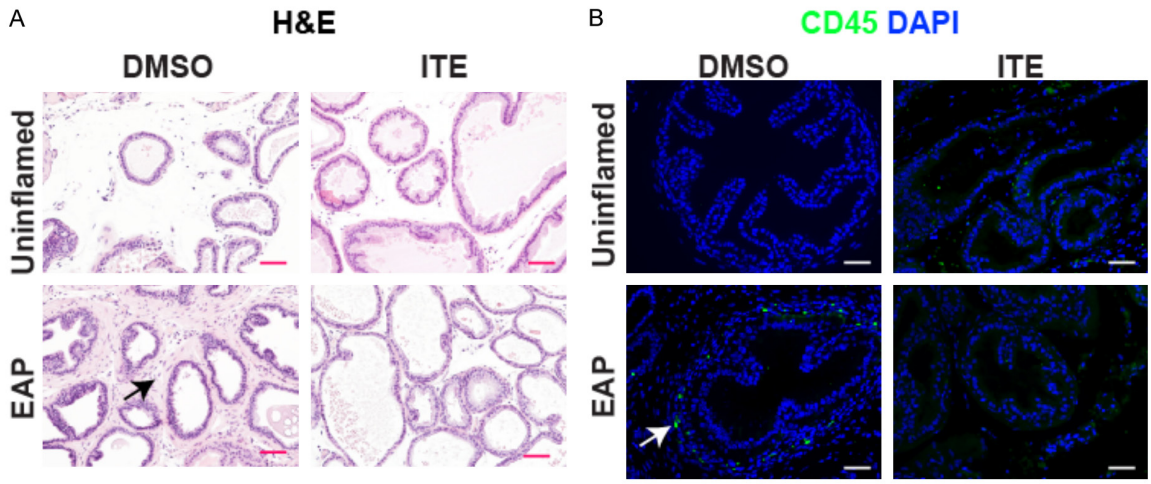

Figure 2. ITE protects against an EAP mediated increase in dorsal prostate inflammation. EAP was induced and mice were treated with ITE or DMSO (vehicle) as described in **Figure 1** and dorsal prostate tissue was collected seven days after induction of EAP and 5 μm formalin fixed, paraffin embedded tissue sections were prepared. A. Tissue sections were stained with hematoxylin and eosin. Note the thickened periductal stromal cellularity in EAP mice (black arrow) and that ITE appears to protect against this histological change which is normally associated with inflammation. B. Tissue sections were labeled with an antibody against CD45 (green, labels leukocytes) and stained with DAPI (blue) to visualize nuclei. Note the green CD45+ cells (white arrow) that appear to be more abundant in the lower left panel than in other panels. Results are representative of three mice per group. Scale bars are 100 microns.

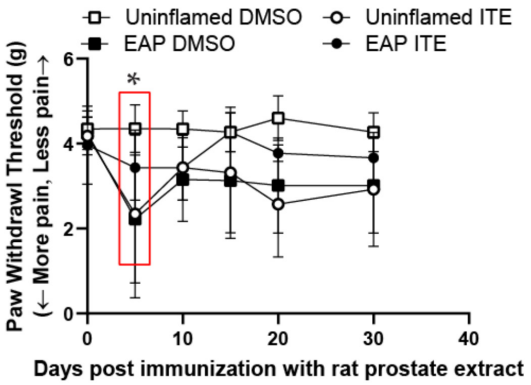

Figure 3. ITE protects against EAP mediated allodynia. EAP was induced and mice were treated with ITE or DMSO (vehicle) as described in **Figure 1**. Von Frey filaments of increasing stiffness were incrementally applied to the lateral glabrous skin of the hind paw, every 5 days, to determine the amount of force required to induce paw withdrawal. Von Frey testing was repeated for a duration of 30 days. Results are mean ± SEM of three mice/group. The results were not normally distributed and differences between groups were determined using a Kruskal-Wallis. An Asterisk indicates a significant difference ($P < 0.05$) between groups.

ITE reduces changes in micturition behavior induced by EAP

Prostate inflammation has been linked to changes in voiding behaviors like urinary retention and polyuria [26, 27]. We conducted void spot assays, 6 days after immunization, to determine whether EAP drives changes in mouse voiding behavior and whether ITE protects against these changes. Mice were placed in cages lined with filter paper for 4 hours and urine was visualized with UV transillumination (**Figure 4A**). We assessed urine spot number, spot size, total urine area, primary void area, corner, and center voiding (**Figure 4B**). There were more void spots in EAP ITE mice ($P = 0.0015$) than in any other group. There were no significant differences among groups in the total voided urine area or the spatial distribution of urine spots (spots in the center versus in the corners) (**Figure 4B**). We used anesthetized cystometry to evaluate the bladder response to filling and emptying. Cystometry was completed 6 days after immunization. Representative cystometrograms are shown in **Figure 4C**. EAP appeared to increase the number of non-voiding contractions and ITE appeared to protect against this change (**Figure 4D**).

ITE protects against EAP-mediated increases in H2-ab1, S100a8, and S100a9 RNA abundance in the dorsal prostate

We conducted NanoString nCounter multiplex gene expression analysis using the inflamma-

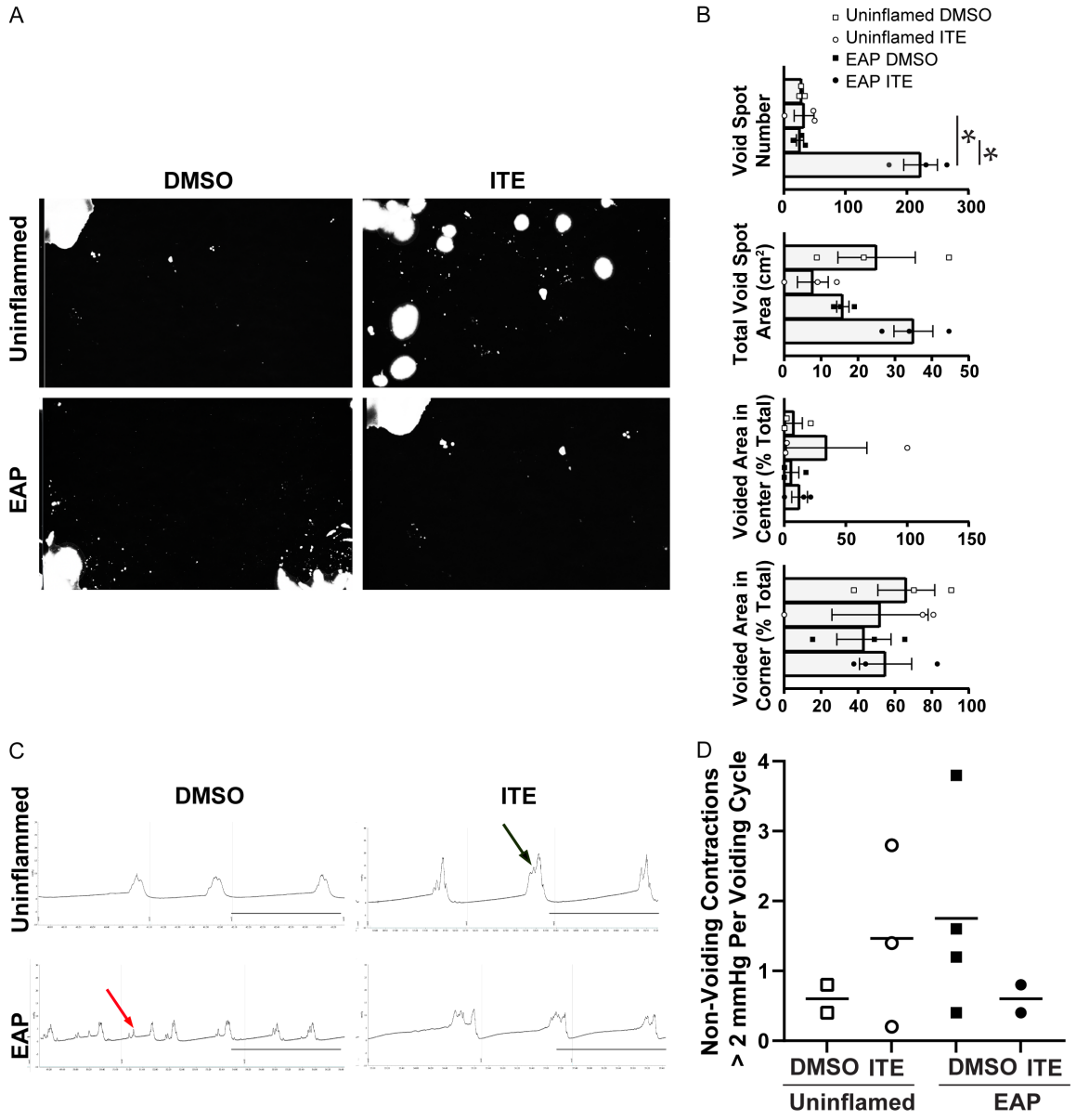

Figure 4. ITE protects against EAP mediated changes to voiding behavior. EAP was induced and mice were treated with ITE or DMSO (vehicle) as described in **Figure 1** and voiding behavior was evaluated on day 7. The void spot assay (VSA) was used to quantify spontaneous voiding behavior. Mice were tested for 4 hours in cages lined with WhatmanÒ cellulose filter paper. (A) Representative voiding patterns. (B) Void spot number, total void spot area, voided area in the center of the cage, and voided area in the corner of the cage were quantified. Results are mean ± SEM, 3 mice per group. A Shapiro-Wilk test confirmed normality of distribution ($P < 0.05$) and differences between groups were determined using a one-way Analysis of Variance (ANOVA) followed by Tukey Multiple Comparisons Test. Asterisks indicate significant difference between groups ($P < 0.05$). (C) Mice were anesthetized, a cystostomy catheter was passed through the bladder dome, and saline was infused at a rate of 0.8 milliliters/hour while continuously measuring bladder pressure in response to filling and emptying. Representative pressure versus time traces are shown. Intravesical pressures (mmHg) are shown on the y-axis. Scale bars: 2.5 min. The black arrow indicates bladder contractions during a voiding event and the red arrow indicates non-voiding contractions. (D) Non-voiding contractions were quantified, results are mean ± SEM, 3 mice per group for (A, B) and 2-4 mice per group for (C, D).

tion panel to identify EAP-mediated changes in dorsal prostate RNA abundance that were mitigated by ITE. Prostates were collected 6 d after immunization for NanoString analysis. A total of 561 unique inflammation related RNAs were quantified and EAP significantly reduced abun-

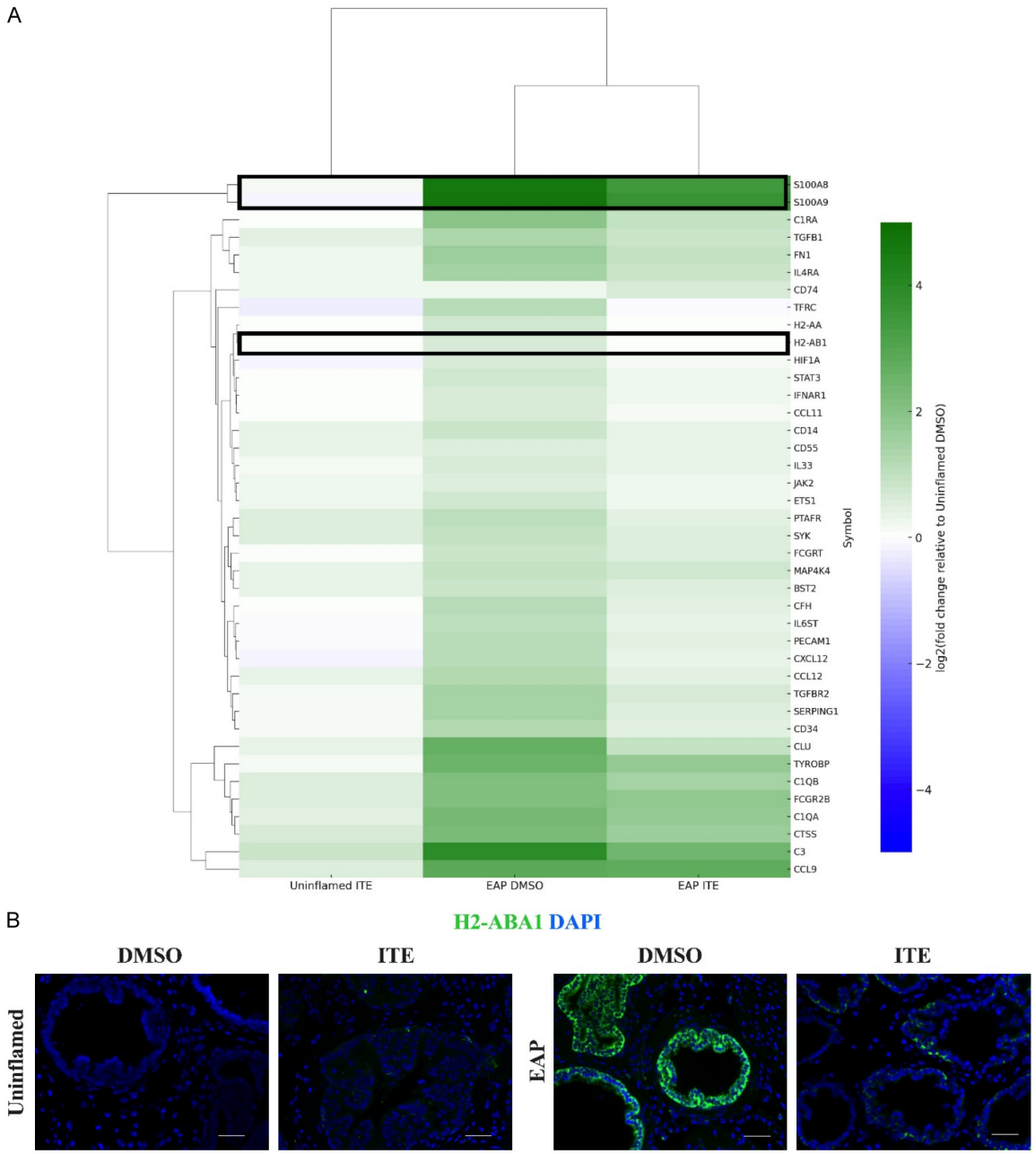

Figure 5. ITE protects against some EAP mediated changes in inflammatory gene expression. EAP was induced and mice were treated with ITE or DMSO (vehicle) as described in **Figure 1** and dorsal prostate tissue was collected seven days after induction of EAP. A. The Nanostring nCounter Inflammation panel was used to evaluate inflammatory gene expression. ITE protected against an EAP mediated increase in a cluster of RNAs which included *H2-ab1*. B. Tissue sections were labeled with an RNAScope™ probe against *H2-ab1* (green) and stained with DAPI (blue) to visualize nuclei. Results are representative of three mice per group. Scale bars are 100 micron.

dance of 10 RNAs and increased abundance of 30 RNAs. We performed k-means clustering on differentially expressed genes to pinpoint EAP mediated gene expression changes that were counteracted by ITE (**Figure 5A**). S100 calcium-binding protein A9 (*S100a9*) encodes a subunit of the protein calprotectin, an abundant protein in neutrophils, and were highly induced by EAP, and ITE protected against the EAP-mediated increase (**Figure 5A**). Histocompatibility 2, class II antigen A (*H2-ab1*) encodes an antigen processing protein which is orthologous to the

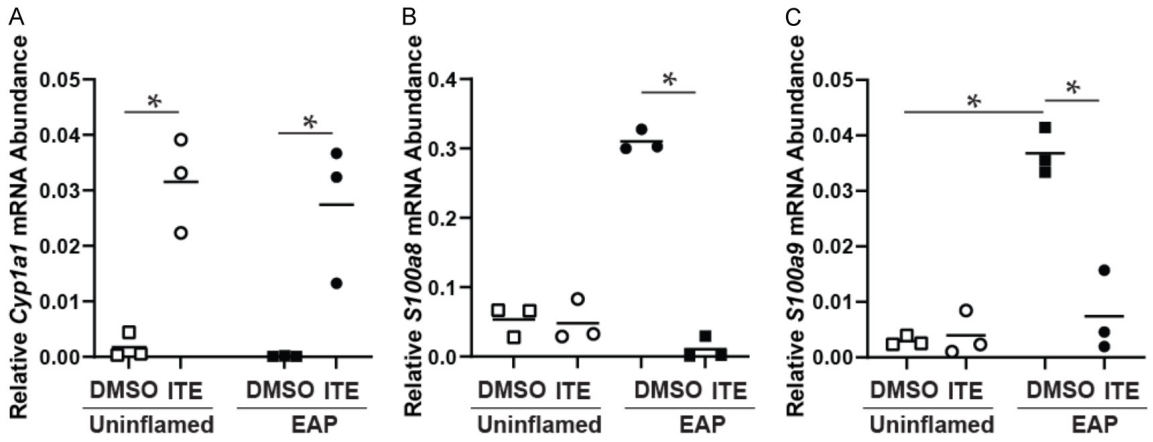

Figure 6. EAP induces calprotectin subunits *S100a8* and *S100a9* and ITE significantly reduces these increases. EAP was induced and mice were treated with ITE or DMSO (vehicle) as described in **Figure 1** and prostate tissue was collected four hours later. The relative abundance of (A) *Cyp1a1*, (B) *S100a8*, and (C) *S100a9* were determined and normalized to the abundance of peptidyl prolyl isomerase A (*Ppia*). Results are mean ± SEM, 3 mice per group. A Shapiro-Wilk test confirmed normality of distribution ($P < 0.05$) (A and C) were normally distributed and differences between groups were determined using a one-way Analysis of Variance (ANOVA) followed by Tukey Multiple Comparisons Test. (B) was not normally distributed and differences between groups were determined using a Kruskal-Wallis Test followed by Dunn's Multiple Comparisons Test. Asterisks indicate significant difference between groups ($P < 0.05$).

human major histocompatibility complex, class II, DQ beta 2, and which has been linked to inflammation and autoimmunity [28]. EAP increased the abundance of *H2-ab1* RNA and ITE protected against this increase (**Figure 5A**). To independently validate this observation, we used RNAScope™ to label dorsal prostate tissue sections from each of the four experimental groups with a probe against *H2-ab1* (**Figure 5B**). *H2-ab1* was not detected in dorsal prostates of mice without EAP. *H2-ab1* was abundant in dorsal prostate epithelium (basal + luminal epithelium) of EAP mice treated with DMSO but was visibly less abundant in EAP mice treated with ITE, where it was restricted to a subset of basal cells. Why *H2-ab1* remained in some basal cells after ITE treatment is unknown and the significance of this finding is unclear. We also treated mice with rat prostate antigen or adjuvant alone, and then ITE or DMSO vehicle and dorsolateral prostate was collected 4 hours later, RNA was isolated, and the abundance of *Cyp1a1*, a known AHR target gene, was determined to test whether AHR signaling is potentially activated. ITE significantly increased the relative abundance of *Cyp1a1* (**Figure 6A**). EAP also significantly increased the abundance of *S100a8* and *S100a9*, and ITE protected against the EAP-mediated increase (**Figure 6B**, **6C**).

Discussion

Prostate autoimmunity has been linked to several benign prostatic diseases but there are no medications currently approved to target this disease mechanism. The goal of this study was to leverage recent findings that AHR activation can reduce autoimmune-mediated inflammation in a variety of tissues and test whether the AHR agonist, ITE, reduces prostate inflammation. We collected histological, physiological, and molecular evidence that supports an ITE-mediated reduction of inflammation, pain, and voiding dysfunction in a mouse model of EAP.

In humans, prostatic inflammation is suggested to activate efferent neural pathways, consequently precipitating a localized nociceptive response through the activation of dorsal root ganglia neurons [29]. We observed that induction of EAP reduces the withdrawal threshold to Von Frey filaments, consistent with tactile allodynia, and this phenotype is mitigated by the treatment with ITE 5 days post immunization but not at later time points. This observation aligns with clinical manifestations in humans where the intensity of pain correlates with the frequency of symptomatic episodes, such as dysuria and dysorgasmia (painful ejaculation), intimating that the acuteness of nociception is

exacerbated during peak inflammatory states [30]. A potential limitation of this model stems from its utilization of the C57BL/6J mouse strain, noted for its comparatively subdued immune response relative to other strains [31], which might influence the generalizability of the findings.

We used the NanoString nCounter inflammation panel to identify gene expression changes driven by autoimmune prostatitis and blocked by ITE as a first step in understanding the ITE mechanism of action. We found that autoimmune prostatitis increased *H2-ab1* RNA in prostate epithelial cells and that ITE prevented the increase. Mucosal epithelial cells, such as those in the gut, use MHC II molecules, including H2-AB1, to activate CD4+ T effector cells [32] and to facilitate self-renewal of epithelium [33]. H2-AB1 abundance in intestinal epithelial cells increases in response to inflammation and autoimmunity [34-36]. H2-AB1 is required for inflammation in a mouse model of allergic rhinitis [37] and is required in a mouse model of graft versus host disease [38]. A previous study also demonstrated the requirement for H2-AB1 in autoimmune prostatitis in non-obese diabetic mice [38]. AHR activation ligands more potent than ITE, were previously shown to increase *H2-ab1* abundance in non-inflammatory research models involving jejunal epithelial cells and liver [39, 40]. Though we specifically observed an ITE mediated decrease in *H2-ab1* abundance in this study, our model involved inflammation and a different ligand. It would be worthwhile to investigate whether *H2-ab1* is required for the inhibitory actions of ITE on autoimmune prostatitis.

EAP increased the abundance of *S100a8* and *S100a9* RNAs, which encode peptides that assemble into calprotectin. ITE blocked the EAP mediated increase in *S100a8* and *S100a9*. Calprotectin plays a crucial role in controlling inflammation, especially in autoimmune diseases [41, 42]. This protein not only regulates inflammatory responses by acting as a damage-associated molecular pattern molecule that attracts leukocytes to inflammation sites but is also pivotal in the body's defense against pathogens [42]. Elevated calprotectin abundance has been linked to the severity of rheumatoid arthritis [43], inflammatory bowel disease [44], and psoriasis [43], indicating its significant impact on the pathology of these disorders [45]. The repression of calprotectin may be a mechanism by which ITE reduces prostate inflammation in mice with EAP.

Acknowledgements

The authors gratefully acknowledge the support and resources provided by the Research Animal Resources and Compliance (RARC) Core and Biomedical Research Modeling Services (BRMS), which greatly contributed to the successful completion of this project. We would also like to express our appreciation to the University of Wisconsin O'Brien Center Rodent Urinary Function Testing Core. This work was funded by National Institutes of Health grants R01 ES001332, R00 ES029537, T32 ES007015 and U54 DK104310. The content is solely the responsibility of the authors and does not necessarily represent the official views of the National Institutes of Health. This work does not represent the views of the Department of Veterans Affairs or the United States Government.

Disclosure of conflict of interest

None.

Address correspondence to: Dr. Chad M Vezina, Department of Comparative Biosciences, University of Wisconsin-Madison, 1656 Linden Drive, Hanson Biomedical Sciences Laboratory, Madison, WI 53705, USA. Tel: 608-890-3235; E-mail: cmvezina@wisc.edu

References

[1] Duloy AM, Calhoun EA and Clemens JQ. Economic impact of chronic prostatitis. Curr Urol Rep 2007; 8: 336-339.

[2] Welliver C, Feinstein L, Ward JB, Kirkali Z, Martinez-Miller E, Matlaga BR and McVary K; Urologic Diseases in America Project. Evolution of healthcare costs for lower urinary tract symptoms associated with benign prostatic hyperplasia. Int Urol Nephrol 2022; 54: 2797-2803.

[3] Chen L, Zhang M and Liang C. Chronic prostatitis and pelvic pain syndrome: another autoimmune disease? Arch Immunol Ther Exp (Warsz) 2021; 69: 24.

[4] Zhang Y, Li X, Zhou K, Zhou M, Xia K, Xu Y, Sun X, Zhu Y, Cui C and Deng C. Influence of experimental autoimmune prostatitis on sexual function and the anti-inflammatory efficacy of celecoxib in a rat model. Front Immunol 2020; 11: 574212.

[5] Liu Y, Wazir J, Tang M, Ullah R, Chen Y, Chen T and Zhou X. Experimental autoimmune prostatitis: different antigens induction and antigen-specific therapy. Int Urol Nephrol 2021; 53: 607-618.
[6] Vinnik YY, Kuzmenko AV and Gyaurgiev TA. Treatment of the chronic prostatitis: current state of the problem. Urologiia 2021; 4: 138-144.
[7] Vickman RE, Aaron-Brooks L, Zhang R, Lanman NA, Lapin B, Gil V, Greenberg M, Sasaki T, Cresswell GM, Broman MM, Paez JS, Petkewicz J, Talaty P, Helfand BT, Glaser AP, Wang CH, Franco OE, Ratliff TL, Nastiuk KL, Crawford SE and Hayward SW. TNF is a potential therapeutic target to suppress prostatic inflammation and hyperplasia in autoimmune disease. Nat Commun 2022; 13: 2133.
[8] Liedtke V, Stöckle M, Junker K and Roggenbuck D. Benign prostatic hyperplasia - a novel autoimmune disease with a potential therapy consequence? Autoimmun Rev 2024; 23: 103511.
[9] Rikken G, van den Brink NJM, van Vlijmen-Willems IMJJ, van Erp PEJ, Pettersson L, Smits JPH and van den Bogaard EH. Carboxamide derivatives are potential therapeutic AHR ligands for restoring IL-4 mediated repression of epidermal differentiation proteins. Int J Mol Sci 2022; 23: 1773.
[10] Rothhammer V, Mascanfroni ID, Bunse L, Takenaka MC, Kenison JE, Mayo L, Chao CC, Patel B, Yan R, Blain M, Alvarez JI, Kébir H, Anandasabapathy N, Izquierdo G, Jung S, Obholzer N, Pochet N, Clish CB, Prinz M, Prat A, Antel J and Quintana FJ. Type I interferons and microbial metabolites of tryptophan modulate astrocyte activity and central nervous system inflammation via the aryl hydrocarbon receptor. Nat Med 2016; 22: 586-597.
[11] Gupta A, Gupta S, Pavuk M and Roehrborn CG. Anthropometric and metabolic factors and risk of benign prostatic hyperplasia: a prospective cohort study of Air Force veterans. Urology 2006; 68: 1198-1205.
[12] Gupta A, Ketchum N, Roehrborn CG, Schecter A, Aragaki CC and Michalek JE. Serum dioxin, testosterone, and subsequent risk of benign prostatic hyperplasia: a prospective cohort study of Air Force veterans. Environ Health Perspect 2006; 114: 1649-1654.
[13] Gupta A, Schecter A, Aragaki CC and Roehrborn CG. Dioxin exposure and benign prostatic hyperplasia. J Occup Environ Med 2006; 48: 708-714.
[14] Song J, Clagett-Dame M, Peterson RE, Hahn ME, Westler WM, Sicinski RR and DeLuca HF. A ligand for the aryl hydrocarbon receptor isolated from lung. Proc Natl Acad Sci U S A 2002; 99: 14694-14699.
[15] Henry EC, Bemis JC, Henry O, Kende AS and Gasiewicz TA. A potential endogenous ligand for the aryl hydrocarbon receptor has potent agonist activity in vitro and in vivo. Arch Biochem Biophys 2006; 450: 67-77.
[16] Rudick CN, Schaeffer AJ and Thumbikat P. Experimental autoimmune prostatitis induces chronic pelvic pain. Am J Physiol Regul Integr Comp Physiol 2008; 294: R1268-1275.
[17] Wegner KA, Abler LL, Oakes SR, Mehta GS, Ritter KE, Hill WG, Zwaans BM, Lamb LE, Wang Z, Bjorling DE, Ricke WA, Macoska J, Marker PC, Southard-Smith EM, Eliceiri KW and Vezina CM. Void spot assay procedural optimization and software for rapid and objective quantification of rodent voiding function, including overlapping urine spots. Am J Physiol Renal Physiol 2018; 315: F1067-F1080.
[18] Keil KP, Abler LL, Laporta J, Altmann HM, Yang B, Jarrard DF, Hernandez LL and Vezina CM. Androgen receptor DNA methylation regulates the timing and androgen sensitivity of mouse prostate ductal development. Dev Biol 2014; 396: 237-245.
[19] Gonzalez-Cano R, Boivin B, Bullock D, Cornelissen L, Andrews N and Costigan M. Up-down reader: an open source program for efficiently processing 50% von frey thresholds. Front Pharmacol 2018; 9: 433.
[20] Kennedy CL, Spiegelhoff A, Lavery T, Wang K, Manuel RS, Wang Z, Wildermuth H and Keil Stietz KP. Developmental polychlorinated biphenyl (PCB) exposure alters voiding physiology in young adult male and female mice. Am J Clin Exp Urol 2022; 10: 82-97.
[21] Perkins JR, Dawes JM, McMahon SB, Bennett DL, Orengo C and Kohl M. ReadqPCR and NormqPCR: R packages for the reading, quality checking and normalisation of RT-qPCR quantification cycle (Cq) data. BMC Genomics 2012; 13: 296.
[22] Rivero VE, Motrich RD, Maccioni M and Riera CM. Autoimmune etiology in chronic prostatitis syndrome: an advance in the understanding of this pathology. Crit Rev Immunol 2007; 27: 33-46.
[23] Hou Y, DeVoss J, Dao V, Kwek S, Simko JP, McNeel DG, Anderson MS and Fong L. An aberrant prostate antigen-specific immune response causes prostatitis in mice and is associated with chronic prostatitis in humans. J Clin Invest 2009; 119: 2031-2041.
[24] Yue T, Sun F, Yang C, Wang F, Luo J, Yang P, Xiong F, Zhang S, Yu Q and Wang CY. The AHR signaling attenuates autoimmune responses during the development of type 1 diabetes. Front Immunol 2020; 11: 1510.

[25] Breser ML, Salazar FC, Rivero VE and Motrich RD. Immunological mechanisms underlying chronic pelvic pain and prostate inflammation in chronic pelvic pain syndrome. Front Immunol 2017; 8: 898.
[26] Nickel JC. Prostatitis. Can Urol Assoc J 2011; 5: 306-315.
[27] Toh KL and Ng CK. Urodynamic studies in the evaluation of young men presenting with lower urinary tract symptoms. Int J Urol 2006; 13: 520-523.
[28] Maglakelidze N, Gao T, Feehan RP and Hobbs RP. AIRE deficiency leads to the development of alopecia areata-like lesions in mice. J Invest Dermatol 2023; 143: 578-587, e3.
[29] He H, Luo H, Qian B, Xu H, Zhang G, Zou X and Zou J. Autonomic nervous system dysfunction is related to chronic prostatitis/chronic pelvic pain syndrome. World J Mens Health 2024; 42: 1-28.
[30] Wagenlehner FM, van Till JW, Magri V, Perletti G, Houbiers JG, Weidner W and Nickel JC. National institutes of health chronic prostatitis symptom index (NIH-CPSI) symptom evaluation in multinational cohorts of patients with chronic prostatitis/chronic pelvic pain syndrome. Eur Urol 2013; 63: 953-959.
[31] Zhang Q, Zhu W, Zou Z, Yu W, Gao P, Wang Y and Chen J. A preliminary study in immune response of BALB/c and C57BL/6 mice with a locally allergic rhinitis model. Am J Rhinol Allergy 2023; 37: 410-418.
[32] Dotan I, Allez M, Nakazawa A, Brimnes J, Schulder-Katz M and Mayer L. Intestinal epithelial cells from inflammatory bowel disease patients preferentially stimulate CD4+ T cells to proliferate and secrete interferon-gamma. Am J Physiol Gastrointest Liver Physiol 2007; 292: G1630-1640.
[33] Heuberger C, Pott J and Maloy KJ. Why do intestinal epithelial cells express MHC class II? Immunology 2021; 162: 357-367.
[34] Lorenzo G, Scott MA, Tew K, Hughes TJ, Zhang YJ, Liu L, Vilanova G and Gomez H. Tissue-scale, personalized modeling and simulation of prostate cancer growth. Proc Natl Acad Sci U S A 2016; 113: E7663-E7671.
[35] Koyama M, Mukhopadhyay P, Schuster IS, Henden AS, Hülsdünker J, Varelias A, Vetizou M, Kuns RD, Robb RJ, Zhang P, Blazar BR, Thomas R, Begun J, Waddell N, Trinchieri G, Zeiser R, Clouston AD, Degli-Esposti MA and Hill GR. MHC class II antigen presentation by the intestinal epithelium initiates graft-versus-host disease and is influenced by the microbiota. Immunity 2019; 51: 885-898, e7.
[36] Kelly J, Weir DG and Feighery C. Differential expression of HLA-D gene products in the normal and coeliac small bowel. Tissue Antigens 1988; 31: 151-160.
[37] Tang Z, Wang Y, Lv L, Li L and Zhang H. Mice with double knockout of H2-Eb1 and H2-Ab1 exhibit reduced susceptibility to allergic rhinitis. PLoS One 2018; 13: e0206122.
[38] Covassin L, Laning J, Abdi R, Langevin DL, Phillips NE, Shultz LD and Brehm MA. Human peripheral blood CD4 T cell-engrafted non-obese diabetic-scid IL2rγ(null) H2-Ab1 (tm1Gru) Tg (human leucocyte antigen D-related 4) mice: a mouse model of human allogeneic graft-versus-host disease. Clin Exp Immunol 2011; 166: 269-280.
[39] Fader KA, Nault R, Ammendolia DA, Harkema JR, Williams KJ, Crawford RB, Kaminski NE, Potter D, Sharratt B and Zacharewski TR. 2,3,7,8-tetrachlorodibenzo-p-dioxin alters lipid metabolism and depletes immune cell populations in the jejunum of C57BL/6 mice. Toxicol Sci 2015; 148: 567-580.
[40] Boverhof DR, Burgoon LD, Tashiro C, Sharratt B, Chittim B, Harkema JR, Mendrick DL and Zacharewski TR. Comparative toxicogenomic analysis of the hepatotoxic effects of TCDD in Sprague Dawley rats and C57BL/6 mice. Toxicol Sci 2006; 94: 398-416.
[41] Xu YD, Wang Y, Yin LM, Park GH, Ulloa L and Yang YQ. S100A8 protein attenuates airway hyperresponsiveness by suppressing the contraction of airway smooth muscle. Biochem Biophys Res Commun 2017; 484: 184-188.
[42] Carnazzo V, Redi S, Basile V, Natali P, Gulli F, Equitani F, Marino M and Basile U. Calprotectin: two sides of the same coin. Rheumatology (Oxford) 2024; 63: 26-33.
[43] Huang JX, Lee YH, Ko MY and Wei JC. Calprotectin in psoriatic arthritis: inflammation and beyond. Int J Rheum Dis 2023; 26: 11-12.
[44] Khaki-Khatibi F, Qujeq D, Kashifard M, Moein S, Maniati M and Vaghari-Tabari M. Calprotectin in inflammatory bowel disease. Clin Chim Acta 2020; 510: 556-565.
[45] Wang S, Song R, Wang Z, Jing Z, Wang S and Ma J. S100A8/A9 in inflammation. Front Immunol 2018; 9: 1298.